Journal of Catalysis **210,** 431–444 (2002)
doi:10.1006/jcat.2002.3691

Kinetics and Mechanisms of *n*-Propylbenzene Hydrodealkylation Reactions over Pt(Sn)/SiO_2 and (Cl–)Al_2O_3 Catalysts in Reforming Conditions

Stéphanie Toppi,*,† Cyril Thomas,* Céline Sayag,* Dominique Brodzki,* Fabienne Le Peltier,† Christine Travers,† and Gérald Djéga-Mariadassou[1]

*Laboratoire de Réactivité de Surface, UMR CNRS 7609, Université Pierre et Marie Curie, 4 Place Jussieu, 75252 Paris Cedex 05, France; and †Institut Français du Pétrole, 1 et 4 Avenue de Bois-Préau, 92852 Rueil-Malmaison Cedex, France

Received March 11, 2002; revised May 24, 2002; accepted May 24, 2002

Kinetics of *n*-propylbenzene hydrodealkylation (HDA) was investigated over model catalysts under reforming operating conditions (773 K, 5 bars, and $H_2/HC = 5$). Silica-supported platinum catalysts (Pt/SiO_2 and $PtSn/SiO_2$) and alumina materials (Al_2O_3 and 1 wt% Cl–Al_2O_3) were chosen to evaluate the influence of the metallic and acidic phases on the HDA reactions, respectively. The kinetic study showed (i) that the HDA processes occurred to a significant extent over both catalytic phases under identical operating conditions and (ii) that hydrodealkylated products (benzene, toluene, and ethylbenzene) were formed through concurrent pathways whatever the nature of the catalytic phase. In addition, product intermediates were identified and mechanisms were suggested to explain the HDA reactions over either different patches of metallic sites or different acid sites (Brønsted and Lewis). Finally, as compared to toluene and ethylbenzene, the formation rate of benzene was the highest over the acidic function and the lowest over Pt/SiO_2.

Key Words: **kinetics; mechanisms; *n*-propylbenzene; hydrodealkylation; hydrogenolysis; cracking; Pt/SiO_2 and $PtSn/SiO_2$ catalysts; chlorinated alumina; reforming; benzene.**

1. INTRODUCTION

Content of aromatic compounds in gasoline has increased both because of the high octane number of aromatic compounds, and because use of tetraethyl lead has been restricted due to environmental concerns. These aromatics (such as benzene, toluene, and xylenes) are mainly provided in the refinery by the reforming unit through the hydrodealkylation (HDA) reaction which consumes hydrogen. However, recent specifications for gasoline drastically limit its aromatic content and new processes have been developed, leading to an aromatic-free gasoline base. In petrochemistry, the demand for aromatics remains strong, and in this case, this operating conditions are adapted to produce high aromatic content; this unit is called an aromizing unit. The refiners' interest is therefore to control and to orientate these HDA reactions depending on the aromatic levels desired.

In both cases (reforming or aromizing), typical reforming catalysts consist of platinum supported on a chlorinated alumina carrier with either tin or rhenium added as promoters. Except for few recent patents (1–4), HDA reactions have scarcely been studied either on bifunctional catalysts or under reforming operating conditions. Indeed, dealkylation reactions have been studied as main reactions in the presence of either steam or hydrogen using supported group VIII metals as catalysts and toluene as a model molecule (5–18). Moreover, all these experiments were carried out at atmospheric pressure and at temperatures ranging from 573 to 773 K (5–18), whereas typical reforming processes are performed from 743 to 803 K with a total pressure ranging from 2.5 to 25 bars. In addition, relatively few studies using alkylbenzenes other than toluene as model molecules are reported in the literature (19–21).

In the work of Grenoble (7), the kinetic study of HDA was considered as a selective hydrogenolysis reaction over alumina-supported platinum catalysts. However, for reforming catalysts that present an acidic function brought about by the chlorinated alumina, the catalytic cracking reaction cannot be ruled out.

In the current paper, the main objective is to evaluate the role of metallic and acidic functions in the kinetics and the mechanisms of HDA of *n*-propylbenzene, (*n*-PB) used as a model molecule. For this purpose, in contrast with previous published results (5–21), this work was carried out under industrial conditions (773 K, 5 bars total pressure, $H_2/HC = 5$) over model catalysts. Silica-supported platinum catalysts with or without tin added as a promoter (Pt/SiO_2 and $PtSn/SiO_2$) were chosen to evaluate the effect of the metallic function on the aromatic distribution, whereas 0 and 1 wt% Cl–Al_2O_3 catalysts were used for the acidic catalysts. It is worth noting that on acid sites HDA is defined

[1] To whom correspondence should be addressed. Fax: 33 1 44 27 60 33. E-mail: djega@ccr.jussieu.fr.

0021-9517/02 $35.00

as a catalytic cracking reaction whereas on metallic sites it is defined as a hydrogenolysis reaction. Particular attention is paid to the influence of either the metallic function (Pt/SiO_2, $PtSn/SiO_2$) or the acidic one (Al_2O_3, $Cl–Al_2O_3$) on the formation of benzene.

2. EXPERIMENTAL

2.1. Materials

GOD 200 γ-Al_2O_3 (BET specific surface area 198 $m^2\ g^{-1}$, grain size 1.0–1.5 mm) and Grace X254 silica (BET specific surface area 540 $m^2\ g^{-1}$, grain size 1–3 mm) were used as supports. The Pt/SiO_2 catalyst (0.5 wt% Pt) was prepared according to the excess impregnation technique for the silica carrier with an ammonia solution of platinum dihydroxotetramine ($Pt(NH_3)_4(OH)_2$, Johnson Matthey). After drying at 353 K overnight, the catalyst was calcined in flowing air (1 L h^{-1} $g^{-1}_{catalyst}$) at 673 K for 2 h and then reduced in flowing hydrogen at 773 K for 2 h. The $PtSn/SiO_2$ catalyst (0.5 wt% Pt and 0.2 wt% Sn) was prepared by impregnation of the Pt/SiO_2 catalyst with an aqueous solution of Me_3SnCl (Aldrich). After drying at 353 K overnight, the catalyst was calcined in flowing air (1 L h^{-1} $g^{-1}_{catalyst}$) at 773 K for 2 h and then reduced in flowing hydrogen at 773 K for 2 h. The 1 wt% chlorinated alumina catalyst was prepared by means of an excess impregnation of the alumina carrier with an aqueous chlorhydric acid solution (1.2 wt% HCl, Merk). After drying at 393 K overnight, the catalyst was calcined in flowing air (1 L $h^{-1}g^{-1}_{catalyst}$) at 773 K for 2 h and then reduced in flowing hydrogen at 773 K for 2 h.

2.2. Catalyst Characterisations

Catalyst characteristics are reported in Table 1. The platinum, tin, and chlorine contents were determined by X-ray fluorescence (Philips PW 1400). The platinum percentage of metal exposed (Pt% ME) measurements were carried out by hydrogen–oxygen titration using a conventional pulsed technique (χ-Sorb Licence IFP). From Table 1, it is shown that the applied protocols allowed the preparation of the desired catalysts and that Pt% ME was 37.5 and 10.5% for Pt/SiO_2 and $PtSn/SiO_2$, respectively. In the case of Pt/SiO_2, the Pt% ME also corresponds to the platinum dispersion, and a mean particle size diameter could be estimated from the following formulae: $D = 0.9/d$, where D and d are the metallic dispersion (%) and the mean particle diameter (nm), respectively (22). This therefore corresponds to a mean particle diameter of 2.4 nm for the unpromoted catalyst. According to the work of Humblot *et al.* (23), a slight increase of the particle size is expected for the tin-promoted catalyst since this latter catalyst was synthesised with the silica-supported platinum catalyst as a starting material, and on which the formation of PtSn alloys was reported in previous studies (23, 24). This latter alloying phenomenon is accountable for the observed decrease in the Pt% ME.

TABLE 1

Composition and Platinum Percentage of Metal Exposed (Pt% ME) of the Synthesised Catalysts

Catalysts	Pt (wt%)	Sn (wt%)	Cl (wt%)	Pt% ME (%)
Pt/SiO_2	0.48	—	—	37.5
$PtSn/SiO_2$	0.48	0.23	—	10.5
Al_2O_3	—	—	—	—
$Cl–Al_2O_3$	—	—	1.00	—

2.3. Kinetic Measurements

A commercial *n*-PB (Fluka, 98% pure) was used as a reactant without any further purification. Liquid *n*-PB was delivered to the catalytic device through a high-pressure piston pump (Gilson 307). The hydrogen flow and the total pressure were controlled by a mass flow controller (Brooks 5850 TR) and back pressure regulator (Brooks 5866), respectively.

Reactions were carried out using 0.8 g of sample in a fixed-bed microreactor at a temperature of 773 K and a total pressure of 5 bars. Kinetic measurements were performed on the stabilised catalysts. The contact time was varied from 0.8 to 4.0 seconds, keeping a hydrogen-to-hydrocarbon molar ratio of 5. The products of reaction were analysed by means of an online gas chromatograph (HP 4890, FID) and the product identification was confirmed by both GC-MS (HP 5890-HP 5971A) analysis and injection of the standards. GC and GC-MS analyses were performed using a PONA (Paraffins-Olefins-Naphthenes-Aromatics) capillary column (length 50 m, inner diameter 0.20 mm, film thickness 0.5 μm).

The absence of diffusion effects on kinetics was verified by the Koros–Nowak criteria (22). Concerning external diffusion, no conversion variation was observed between runs performed with 0.3 and 0.8 g of catalyst with the same contact time. Regarding internal diffusion, no conversion variation was observed by varying the catalyst grain size (0.125–0.160 mm; 0.160–0.200 mm; 0.200–0.250 mm) for a constant weight of catalyst.

3. RESULTS

3.1. Product Distribution over Pt/SiO_2, $PtSn/SiO_2$, Al_2O_3 and 1 wt% $Cl–Al_2O_3$ Catalysts

First, numerous reaction products, for which molecular formulae are reported in Fig. 1, were observed for the *n*-PB conversion (of about 10%), whatever the nature of the catalyst. Using completely different experimental conditions, Shephard and Rooney showed comparable reaction products when studying *n*-PB transformation over an alumina-supported platinum catalyst (19). These products

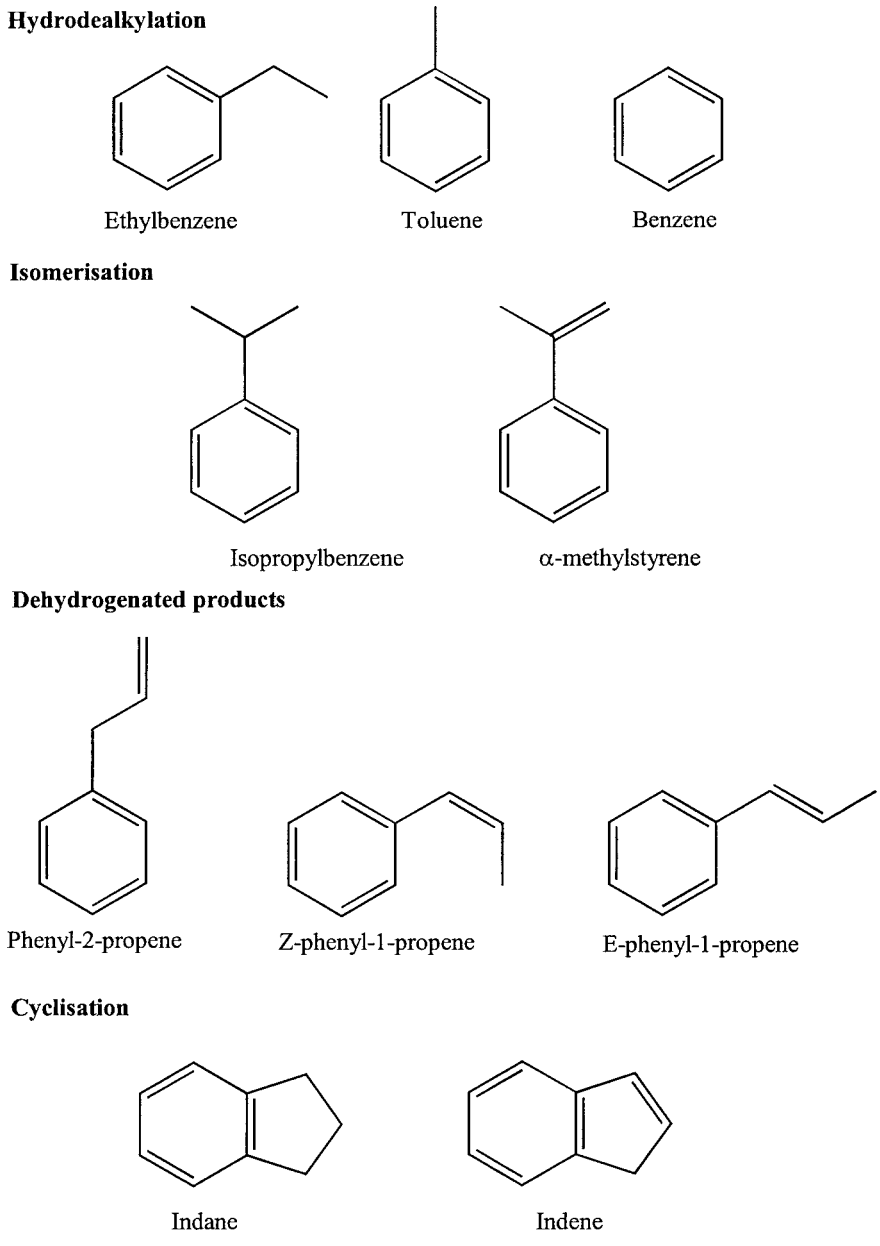

FIG. 1. Molecular formulae of the relevant products observed during *n*-PB conversion at 773 K, 5 bars, and $H_2/HC = 5$.

are gathered into four different family reactions as indicated in Table 2. From this table, it is shown that *n*-PB alkyl chain cyclisation products such as indane and indene are mainly observed on the metallic catalysts and, more particularly, over the unpromoted silica-supported platinum catalyst. In contrast, isopropylbenzene, formed from *n*-PB alkyl chain isomerisation, appears as one of the major products formed on acid sites. Indeed, this isomerisation is a well-known acidic reaction (25). Concerning the dehydrogenated products (phenyl-2-propene, *Z*-phenyl-1-propene, and *E*-phenyl-1-propene), one can see that they are formed on both metallic and acidic functions. The HDA reaction products (benzene, toluene, and ethylbenzene) are also obtained on all catalysts through a C–C bond scission of the alkyl group. On metallic sites, these three products are formed by a hydrogenolysis reaction. In this latter case, benzene exhibits the lower selectivity on the monometallic Pt/SiO_2 catalyst, whereas its selectivity is significantly increased on the promoted catalyst ($PtSn/SiO_2$). On acid sites, the HDA products are formed by catalytic cracking reactions and in this case benzene is the major product over the chlorinated alumina catalyst.

The formation of dehydrogenated products (phenyl-2-propene, *Z*- and *E*-phenyl-1-propene) and HDA products (benzene, toluene, and ethylbenzene) are more specifically studied in the following sections.

TABLE 2

Product Distribution Given as Selectivities at 10% Conversion of *n*-PB (moles of product formed per 100 moles of *n*-PB reacted) on Stabilised Catalysts

Reactions	Products	Pt/SiO_2 (1040)[a]	$PtSn/SiO_2$ (770)[a]	Al_2O_3 (200)[a]	$Cl–Al_2O_3$ (380)[a]
Cyclisation	Indene	5.0	0.0	0.0	0.0
	Indane	31.6	2.6	0.0	0.6
Dehydrogenation	Phenyl-2-propene	2.0	1.8	0.0	0.0
	Z-phenyl-1-propene	4.5	4.4	0.0	2.2
	E-phenyl-1-propene	15.2	16.4	1.4	7.0
Isomerisation	Isopropylbenzene	1.7	4.5	13.0	6.1
	α-Methylstyrene	0.0	0.0	0.0	2.4
	o-Xylene	0.7	1.3	0.0	2.0
	2-Ethyltoluene	2.4	0.0	1.4	0.7
HDA	Methane	10.5	20.6	24.9	11.1
	Ethane	6.4	6.1	14.9	16.5
	Propane	2.9	10.6	8.6	13.2
	Benzene	3.5	13.0	13.0	19.7
	Toluene	6.3	4.7	8.9	7.5
	Ethylbenzene	7.4	14.0	14.0	6.3

[a] Corresponding time on stream (min) of reported data.

3.2. Product Formation versus Time On Stream

3.2.1. Metallic sites contribution (Pt/SiO_2 and $PtSn/SiO_2$). The dehydrogenated and hydrogenolysis product concentrations obtained over Pt/SiO_2 and $PtSn/SiO_2$ catalysts from *n*-PB conversion are reported versus time on stream in Figs. 2 and 3, respectively.

Regarding the dehydrogenated product formation, an identical behaviour is observed in Fig. 2 whatever the catalyst: (i) the concentration of the three products increases with time onstream; (ii) the major product is *E*-phenyl-1-propene, and phenyl-2-propene is the one that displays the lowest concentration; and (iii) the product concentrations are roughly the same on both catalysts (Pt/SiO_2 and $PtSn/SiO_2$). However, steady state is reached a lot more rapidly on the bimetallic catalyst than on the monometallic one, and such a phenomenon is also observed for the hydrogenolysis products (Fig. 3). Concerning these latter products, one can see that their concentrations decrease sharply with time on stream over the unpromoted catalyst (Fig. 3, panel a), due to the metallic phase deactivation, whereas on the promoted catalyst (Fig. 3, panel b), the product concentration is already stable after several minutes on stream. The observed deactivation is attributed to coke deposition over the metallic function. Indeed, a deactivation trend due to sulfur poisoning was ruled out by an additional experiment, not reported in the present study, in which the effect of the sulfur content of the liquid feed was investigated. The comparison between the *n*-PB used in this study (98% purity) and a high-purity *n*-PB (>99%) containing 20 and 2 ppm of sulfur, respectively, was carried out. This comparative study was performed over a

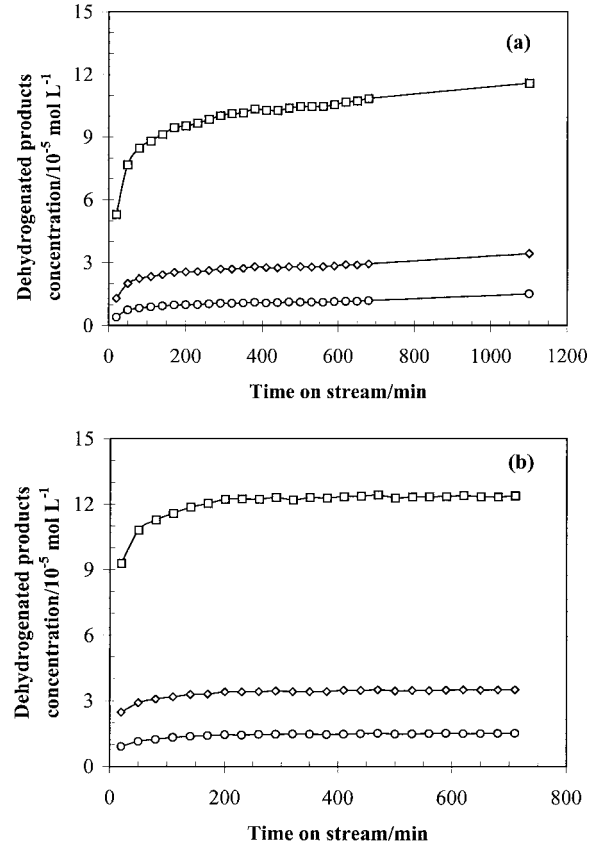

FIG. 2. Concentrations of dehydrogenated products versus time on stream, in *n*-PB conversion at 773 K, 5 bars, and $H_2/HC = 5$: □, *E*-phenyl-1-propene; ◇, *Z*-phenyl-1-propene; and ○, phenyl-2-propene; (a) Pt/SiO_2 and (b) $PtSn/SiO_2$.

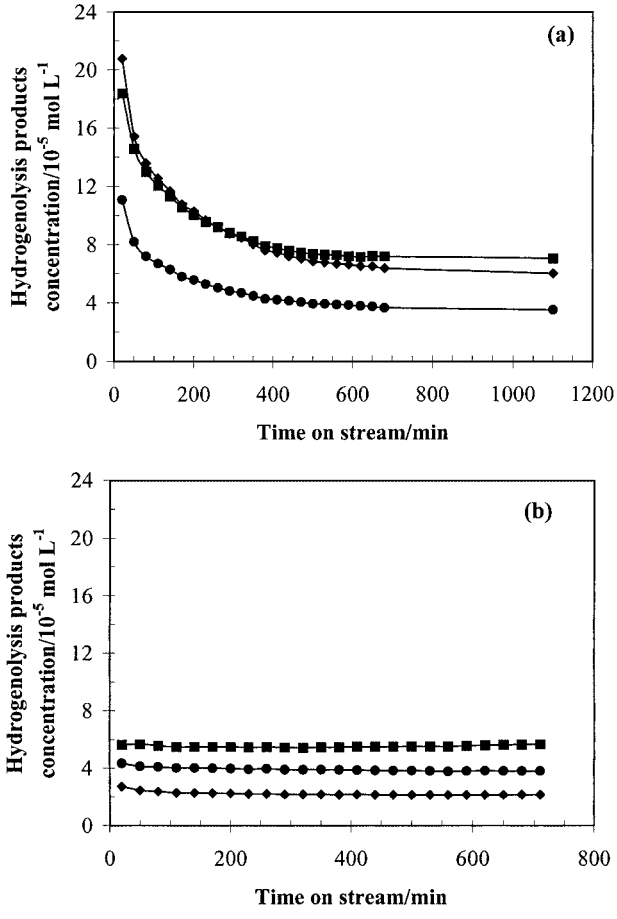

FIG. 3. Concentrations of products of hydrogenolysis versus time on stream, in *n*-PB conversion at 773 K, 5 bars, and $H_2/HC = 5$: ■, ethylbenzene; ◆, toluene; and ●, benzene; (a) Pt/SiO_2 and (b) $PtSn/SiO_2$.

bifunctional catalyst (Pt/Al_2O_3–Cl) to evaluate the impact of sulfur on both metallic and acidic functions. Even with an order of magnitude difference in sulfur content between the two *n*-PB feeds, it was found that the deactivation trend and the product selectivities were the same whatever the sulfur content. The steady state was reached much more rapidly over the tin-promoted catalyst and is therefore attributable to a much lower coking of the latter catalyst as compared to the unpromoted one. Finally, ethylbenzene formation and especially toluene formation occur to lesser extent on $PtSn/SiO_2$ than on Pt/SiO_2 after deactivation. Benzene concentration is the same on both stabilised catalysts (Fig. 3).

3.2.2. Acid sites contribution (Al_2O_3 and 1 wt% Cl–Al_2O_3). The dehydrogenated and catalytic cracking product concentrations obtained over Al_2O_3 and 1 wt%. Cl–Al_2O_3 catalysts from *n*-PB conversion are reported versus time on stream in Figs. 4 and 5, respectively.

Regarding the dehydrogenated products (Fig. 4), only *E*-phenyl-1-propene is detected on Al_2O_3 under our experimental conditions. Figure 4 (panel a) shows that its concentration increases slightly with time on stream. On 1 wt% Cl–Al_2O_3 (Fig. 4, panel b), stable concentrations of *E*- and *Z*-phenyl-1-propene are observed after a rather short period of time on stream; the major product was *E*-phenyl-1-propene.

In the case of the catalytic cracking products (Fig. 5), the aromatic distribution is quite different between the two materials. On Al_2O_3, the concentrations of benzene, toluene, and ethylbenzene are similar (from 3×10^{-5} mol L^{-1} to 5×10^{-5} mol L^{-1}) and ethylbenzene is the major product (Fig. 5, panel a), whereas over 1 wt% Cl–Al_2O_3 (Fig. 5, panel b), benzene is the major product with a much higher concentration (11×10^{-5} mol L^{-1}) than those of toluene and ethylbenzene (around 4×10^{-5} mol L^{-1}).

3.3. Kinetic Results

3.3.1. Reactions over the metallic sites (Pt/SiO_2 and $PtSn/SiO_2$). Dehydrogenated and hydrogenolysis product concentrations obtained over Pt/SiO_2 and $PtSn/SiO_2$ catalysts from *n*-PB conversion versus contact time are

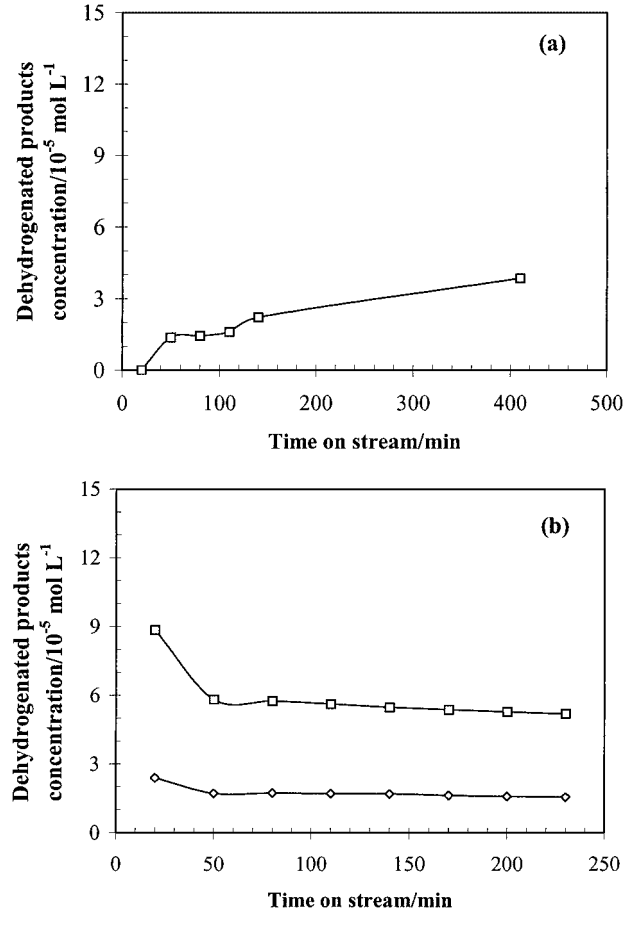

FIG. 4. Concentrations of dehydrogenated products versus time on stream, in *n*-PB conversion at 773 K, 5 bars, and $H_2/HC = 5$: □, *E*-phenyl-1-propene; and ◇, *Z*-phenyl-1-propene; (a) Al_2O_3 and (b) 1 wt% Cl–Al_2O_3.

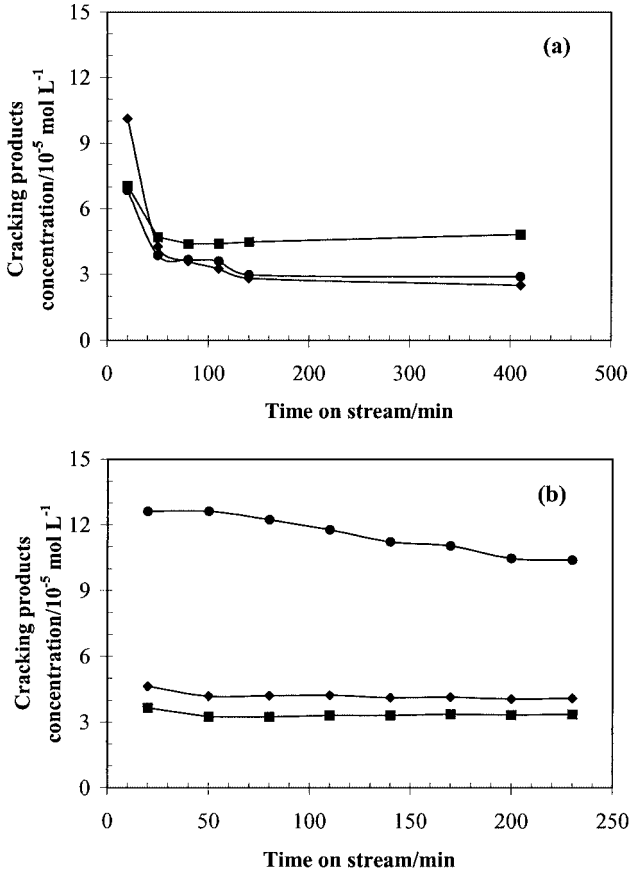

FIG. 5. Concentrations of products of cracking versus time on stream, in *n*-PB conversion at 773 K, 5 bars, and H_2/HC = 5: ■, ethylbenzene; ◆, toluene; and ●, benzene; (a) Al_2O_3 and (b) 1 wt% Cl–Al_2O_3.

shown in Figs. 6 and 7, respectively. The corresponding reaction rates are reported in Table 3.

First, a constant global rate of consumption of *n*-PB is observed over both Pt/SiO_2 and PtSn/SiO_2 catalysts (Fig. 6).

TABLE 3

Dehydrogenation, Hydrogenolysis, or Cracking and Isomerisation Rates of *n*-PB over Different Catalysts at 773 K, 5 bars, and H_2/HC = 5

Products	Reaction rates[a] (10^{-5} mol L^{-1} s^{-1})			
	Pt/SiO_2	PtSn/SiO_2	Al_2O_3	Cl–Al_2O_3
Disappearance rate				
Phenyl-2-propene	0.24	0.12	—	—
Z-phenyl-1-propene	0.44	0.21	—	—
E-phenyl-1-propene	1.04	0.35	—	—
Formation rate				
Benzene	1.43	2.15	3.20	9.82
Toluene	2.26	0.44	1.86	2.94
Ethylbenzene	2.25	1.68	2.64	2.20
Isopropylbenzene	—	—	3.20	3.00

[a] Kinetic data recorded for 8 h of run for metallic catalysts and 5 h of run for nonmetallic catalysts.

Concerning the three products of the dehydrogenation reaction, their concentrations decrease constantly in the range of studied contact times (Fig. 6) and should therefore experience maxima at lower contact times. From Table 3, it can also be observed that the disappearance rates of the dehydrogenated products are from two to three times lower over PtSn/SiO_2 than over Pt/SiO_2.

Regarding the hydrogenolysis products (Fig. 7), it can be seen that the rates of formation of the three products (benzene, toluene, and ethylbenzene) are constant over both silica-supported platinum catalysts. Over Pt/SiO_2, toluene and ethylbenzene are the major products and their formation rates are similar, respectively 2.26×10^{-5} mol L^{-1} s^{-1} and 2.25×10^{-5} mol L^{-1} s^{-1} (Table 3) while benzene is the minor product with a smaller formation rate (1.43×10^{-5} mol L^{-1} s^{-1}). Over the bimetallic catalyst PtSn/SiO_2 (Fig. 7, panel b), the formation rates are affected by the presence of the tin promoter. Indeed, the formation rate of ethylbenzene decreases slightly (1.68×10^{-5} mol L^{-1} s^{-1}) and the formation rate of toluene drops drastically ($0.44 \times$

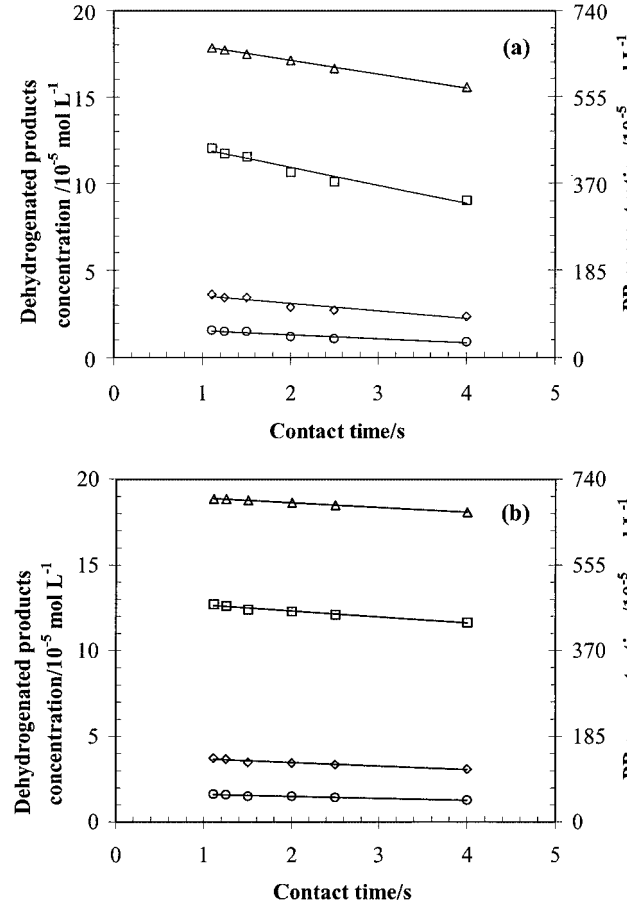

FIG. 6. Concentrations of *n*-PB and dehydrogenated products versus contact time, in *n*-PB conversion at 773 K, 5 bars, and H_2/HC = 5: △, *n*-PB; □, *E*-phenyl-1-propene; ◇, *Z*-phenyl-1-propene; and ○, phenyl-2-propene; (a) Pt/SiO_2 and (b) PtSn/SiO_2. (Kinetic data recorded for 8 h of run.)

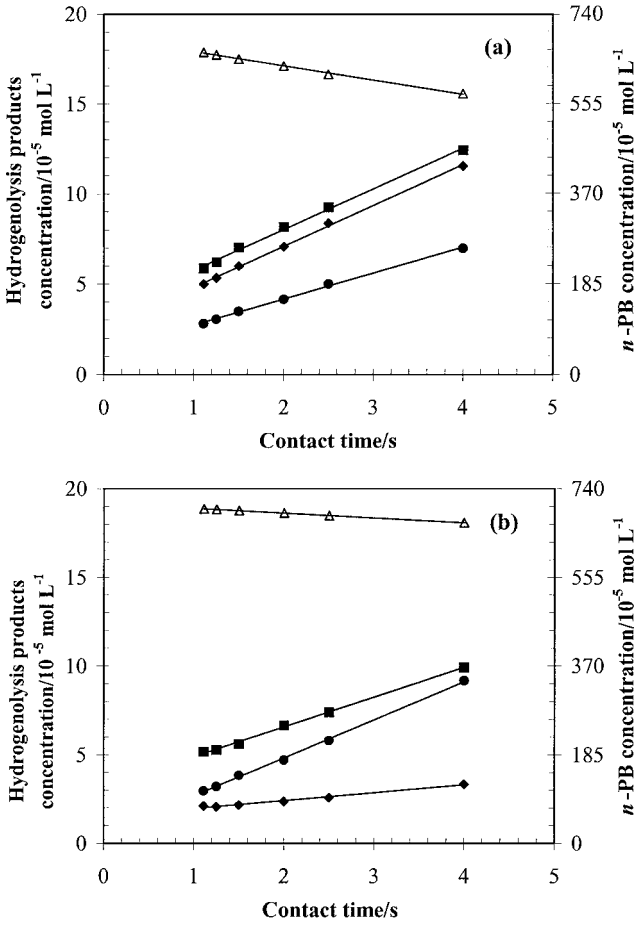

FIG. 7. Concentrations of *n*-PB and products of hydrogenolysis versus contact time, in *n*-PB conversion at 773 K, 5 bars, and $H_2/HC = 5$: △, *n*-PB; ■, ethylbenzene; ◆, toluene; and ●, benzene; (a) Pt/SiO_2 and (b) $PtSn/SiO_2$. (Kinetic data recorded for 8 h of run.)

10^{-5} mol L^{-1} s^{-1}), whereas the formation rate of benzene increases significantly (2.15×10^{-5} mol L^{-1} s^{-1}). Over such a promoted catalyst, toluene thus becomes the minor product.

3.3.2. Reactions over the acid sites (Al_2O_3 and 1 wt% Cl–Al_2O_3). The concentrations of dehydrogenated and catalytic cracking products obtained over Al_2O_3 and 1 wt% Cl–Al_2O_3 catalysts from *n*-PB conversion are shown versus contact time in Figs. 8 and 9, respectively. The corresponding reaction rates are reported in Table 3.

As previously found over the metallic function, the *n*-PB consumption rate is constant over both Al_2O_3 and 1 wt% Cl–Al_2O_3. The formation rates of the dehydrogenated products (Fig. 8) are not constant versus contact time and some discrepancies appear between the two materials in the range of studied contact times. Indeed, over Al_2O_3, *Z*-phenyl-1-propene and *E*-phenyl-1-propene exhibit the same behaviour with an increase of their concentrations up to 1.1 s and a subsequent decrease at higher contact times (Fig. 8, panel a). Over 1 wt% Cl–Al_2O_3, the product concentrations increase and finally seem to reach a plateau (Fig. 8, panel b).

For the catalytic cracking reactions (Fig. 9), the rates of formation of the three products are constant for all catalysts. In the range of the contact times studied, the highest concentration is obtained for ethylbenzene and the lowest for toluene over Al_2O_3. Moreover, the formation rates of both ethylbenzene and toluene are similar (Fig. 9, panel a, and Table 3). In addition, benzene exhibits the highest formation rate (3.20×10^{-5} mol L^{-1} s^{-1}). Such a behaviour is emphasised over 1 wt% Cl–Al_2O_3 with a formation rate of 9.82×10^{-5} mol L^{-1} s^{-1} and in this latter case, benzene becomes the major product. Concerning toluene and ethylbenzene, the formation rates of these two products are significantly affected by chlorine addition. Even though it is not as spectacular as in the case of benzene, it should be noted that the concentration of toluene is higher than that of ethylbenzene over the chlorinated alumina whereas the opposite is observed on alumina (Fig. 9 and Table 3).

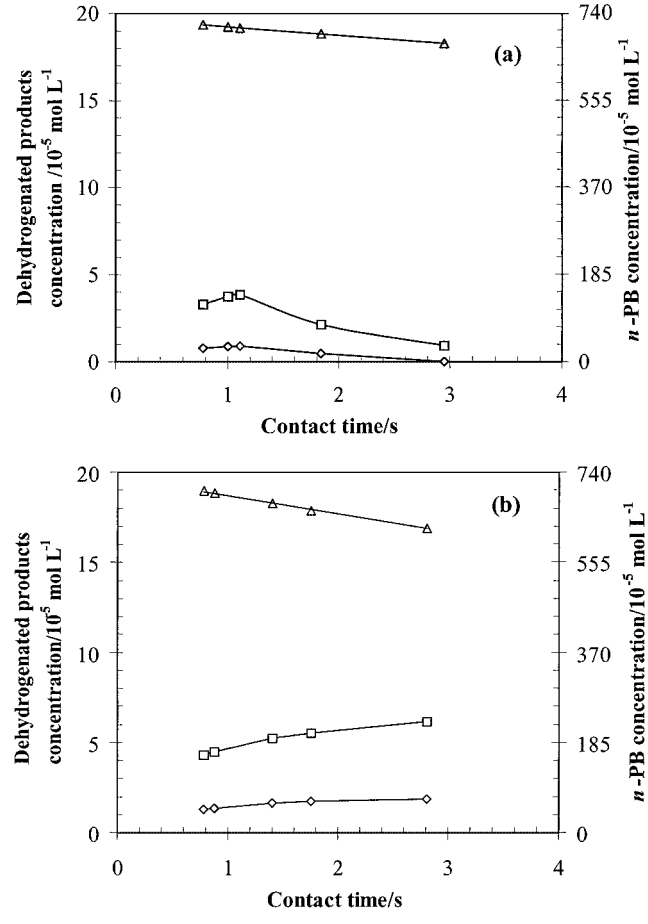

FIG. 8. Concentrations of *n*-PB and dehydrogenated products versus contact time, in *n*-PB conversion at 773 K, 5 bars, and $H_2/HC = 5$: △, *n*-PB; □, *E*-phenyl-1-propene; and ◇, *Z*-phenyl-1-propene; (a) Al_2O_3 and (b) 1 wt% Cl–Al_2O_3. (Kinetic data recorded for 5 h of run.)

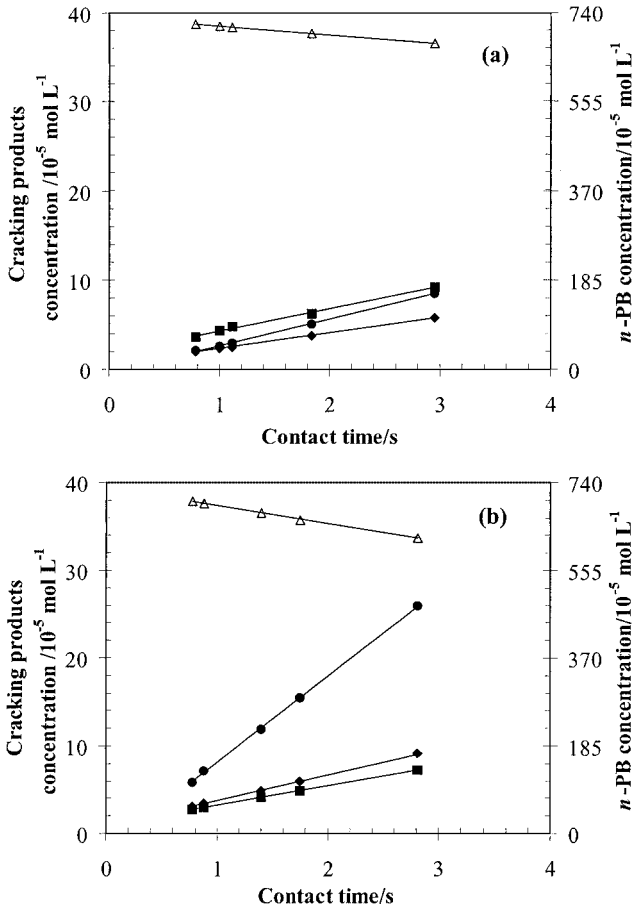

FIG. 9. Concentrations of *n*-PB and products of cracking versus contact time, in *n*-PB conversion at 773 K, 5 bars, and H_2/HC = 5: △, *n*-PB; ■, ethylbenzene; ◆, toluene; and ●, benzene; (a) Al_2O_3 and (b) 1 wt% Cl–Al_2O_3. (Kinetic data recorded for 5 h of run.)

4. DISCUSSION

4.1. Kinetics and Mechanisms over the Metallic Sites (Pt/SiO$_2$ and PtSn/SiO$_2$)

In this section, the global Pt^0 density of sites (Pt^0 being a zero-valent platinum atom) will be denoted as $[L]_M$ and corresponds to the metal dispersion measured according to hydrogen–oxygen titrations.

4.1.1. Zero order reaction with respect to n-PB. Figure 6a indicates that the global rate of consumption of *n*-PB, −d[*n*-PB]/dt, leading to the various detected products, is constant up to 22% conversion of the reactant over Pt/SiO_2. This linear decrease of *n*-PB with contact time, up to such a high conversion value, means that the order related to the *n*-PB is a *true* zero order. It cannot be a degeneracy of the order, which could be assumed if conversion had been less than 10%. This result is presumably due to the experimental conditions. Indeed, pure *n*-PB is sent into the feed with a high partial pressure and therefore saturates all Pt^0 accessible active sites as adsorbed species. Even if a degenerated order could be considered because of the low conversion of the reactant (less than 10%) over PtSn/SiO_2, a true zero order was also assumed over this latter catalyst considering both the experimental conditions (high partial pressure of *n*-PB) and the zero order found over the unpromoted catalyst.

4.1.2. Formation and desorption of phenyl propene species. Since *n*-PB suffers a dehydrogenating chemisorption of the lateral alkyl chain over two adjacent Pt sites, adsorbed phenyl propene species are therefore expected to be the most abundant reactive intermediates (22) on platinum sites. Indeed, phenyl-2-propene, *Z*-phenyl-1-propene, and *E*-phenyl-1-propene were detected in the gas phase over the silica-supported platinum catalysts. For the sake of clarity, phenyl propene species will be denoted as $M_{i,ads}$ when adsorbed and $M_{i,gas}$ when present in the gas phase. Equation [1] can therefore be written as follows with k_1 being the adsorption rate constant of *n*-PB:

$$n\text{-PB}_{gas} \xrightarrow{k_1} M_{i,ads} + H_2. \qquad [1]$$

The one-way arrow presented in Eq. [1] means that the elementary step is far from equilibrium (22), since the dehydrogenation reaction is thermodynamically favoured under the experimental conditions used in this study (773 K, 5 bars, H_2/HC = 5).

The adsorbed phenyl propene species can then desorb, leading to the corresponding species in the gas phase as observed in Fig. 6. Both the formation rates of $M_{i,gas}$ and the desorption rates of $M_{i,ads}$ species are indeed constant due to the saturation of all active sites $[L]_M$ by $M_{i,ads}$ species, as expected from the true zero-order reaction with respect to *n*-PB. Such a behaviour indicates that $M_{i,ads}$ species must be in equilibrium at the surface of the catalyst, while desorbing through a rake mechanism (26), as illustrated in Eq. [2]:

$$\begin{array}{ccccccc} & & M_{1,gas} & & M_{2,gas} & & M_{3,gas} \\ & & \uparrow & & \uparrow & & \uparrow \\ n\text{-PB}_{gas} & \rightarrow & M_{1,ads} & \rightleftarrows & M_{2,ads} & \rightleftarrows & M_{3,ads}. \\ & & L_{1,M} & & L_{2,M} & & L_{3,M} \end{array} \qquad [2]$$

$[L_i]_M$, representing the partial density of sites occupied by $M_{i,ads}$, should be constant and the balance of the metallic sites can therefore be written as follows (Eq. [3]):

$$[L]_M = [L_1]_M + [L_2]_M + [L_3]_M. \qquad [3]$$

For each $M_{i,ads}$ species, the desorption pathway can therefore be summarised as follows:

$$n\text{-PB}_{gas} \xrightarrow{k_1} M_{i,ads} + H_2 \qquad [1]$$

$$M_{i,ads} \xrightarrow{k_{d,i}} M_{i,gas}. \qquad [4]$$

From the kinetic results (Fig. 6, panel b), each desorption rate ($r_{d,i}$) is constant with contact time and is expressed as

follows (step corresponding to Eq. [4]), where $k_{d,i}$ is the corresponding desorption rate constant:

$$r_{d,i} = \frac{\mathrm{d}[\mathrm{M}_{i,\mathrm{gas}}]}{\mathrm{dt}} = k_{d,i}[\mathrm{M}_{i,\mathrm{ads}}] = \text{constant} = k_{d,i}[L_i]_{\mathrm{M}}. \quad [5]$$

Equation [5] confirms that $[L_i]_{\mathrm{M}}$ can be considered as constant, due to the equilibria between surface species (Eq. [2]), since all platinum sites remain saturated under our operating conditions.

4.1.3. Surface reactions of adsorbed phenyl propene species: Hydrogenolysis of C–C bonds of the alkyl chain on Pt^0. Surface reactions of the adsorbed phenyl propene species have to be taken into account to explain the observed decrease of the phenyl propene isomer concentrations reported in Fig. 6. Depending on the contact time, the corresponding adsorbed phenyl propene species can suffer hydrogenolysis reactions, leading to the formation of the dealkylated products reported in Fig. 7. However, the chemical structure of the phenyl propene species can only explain the formation of two out of the three hydrodealkylated products shown in Fig. 7. Indeed, ethylbenzene and toluene are formed through the C–C bond scission of adsorbed phenyl-2-propene and *Z*-/*E*-phenyl-1-propene species, respectively. Therefore *a fourth surface species*, whose corresponding desorbed species was not detected, must be considered to explain the formation of benzene (Fig. 7). This fourth species is either adsorbed on the aromatic nucleus as already suggested by Duprez *et al.* (20) or adsorbed on a single site as assumed by Grenoble (7) and should thus occupy an $L_{4,\mathrm{M}}$ patch of Pt^0 sites to explain the constant formation rate found for benzene (Fig. 7). In addition, the highest concentrations of toluene and ethylbenzene found over the Pt/SiO_2 catalyst (Fig. 7, panel a) are in good agreement with previous studies performed by Duprez *et al.* (20, 21). Indeed, for HDA of *n*-PB over Rh-supported catalysts (20) or HDA of alkylbenzene molecules other than *n*-PB over Pt- and Ni-supported catalysts (21), these authors also reported that the C–C bond scission was favoured in the middle and at the end of the alkyl chain. It is worth noting that the kinetic study of the transformation of a complex molecule such as *n*-PB allowed us to demonstrate that hydrogenolysis reactions follow parallel pathways. Indeed, ethylbenzene, toluene, and benzene are formed concurrently with constant rates at the very beginning of the reaction. In previous studies (7, 12, 13, 16), such a conclusion was not drawn because of the use of toluene as a model molecule which could only lead to the formation of benzene.

The hydrogenolysis pathway can now be summarised as follows where $k_{r,i}$ is the corresponding reaction rate constant:

$$n\text{-PB}_{\mathrm{gas}} \xrightarrow{k_1} \mathrm{M}_{i,\mathrm{ads}} + \mathrm{H}_2 \quad [1]$$

$$\mathrm{M}_{i,\mathrm{ads}} \xrightarrow{k_{r,i}} \mathrm{product}_{i,\mathrm{gas}}. \quad [6]$$

From this pathway and in agreement with experimental results (Fig. 7), the rates of formation of all products can be expressed as follows:

$$r_{\mathrm{product},i} = k_{r,i}[\mathrm{M}_{i,\mathrm{ads}}] = \text{constant} = k_{r,i}[L_i]_{\mathrm{M}}. \quad [7]$$

It has to be emphasised that in the case of zero-order reactions, reaction rates are directly proportional to the number of active sites.

4.1.4. Elementary step sequences of hydrogenolysis reactions and effect of the tin promoter. The kinetic study allows us to suggest reactive intermediates corresponding to the hydrodealkylated products. From the work of Duprez *et al.* (20, 21) and Grenoble (7), benzene formation involves a unique adsorption site (Fig. 10, part a). By extrapolating this afore mentioned elementary step sequence (7) to the formation of toluene and ethylbenzene, it is likely that two adjacent sites are required (Fig. 10, parts b and c). This assumption is fully consistent with both the observed phenyl propene species detected in the gas phase and the formation rates of the hydrodealkylated products reported in Table 3. As expected, the formation rates of ethylbenzene and toluene decrease while that of benzene increases when tin is added as a promoter. Indeed, one of the known effects of tin promotion over silica-supported platinum catalysts is to isolate the zero-valent platinum sites by alloy formation (24, 27, 28) which clearly favours the single-site elementary step sequence leading, in our case, to benzene.

4.2. Mechanisms and Kinetics of n-PB Conversion over the Acid Sites (Al_2O_3 and $Cl–Al_2O_3$)

4.2.1. Acidic mechanism proposals over Al_2O_3 and 1 wt% $Cl–Al_2O_3$. As previously observed on metallic sites (cf. Sect. 4.1.3.), hydrodealkylated products are formed concurrently, according to the constant rates of formation reported in Fig. 9. The direct formation of benzene, toluene, and ethylbenzene on the acid sites was therefore considered through three independent pathways.

Cracking may occur through protolysis (carbonium ions), through a classical chain mechanism (carbenium ions), and finally through a radical process (radical intermediates).

Cracking by protolysis occurs through a monomolecular mechanism involving pentacoordinated intermediates (29) and requires very strong protonic sites such as those found in zeolite-type catalysts. Nevertheless, on Al_2O_3 and 1 wt% $Cl–Al_2O_3$, it is likely that the strength of the protonic sites is not high enough to lead to this mechanism. Therefore either a carbenium ion chain cracking mechanism or a radical process is considered.

Cracking through a carbenium ion chain mechanism is illustrated in Fig. 11 and involves strong Brønsted acid sites. Such strong Brønsted acid sites were already reported over both $Cl–Al_2O_3$ and Al_2O_3 using different probe molecules (30, 31). FTIR adsorption-desorption studies

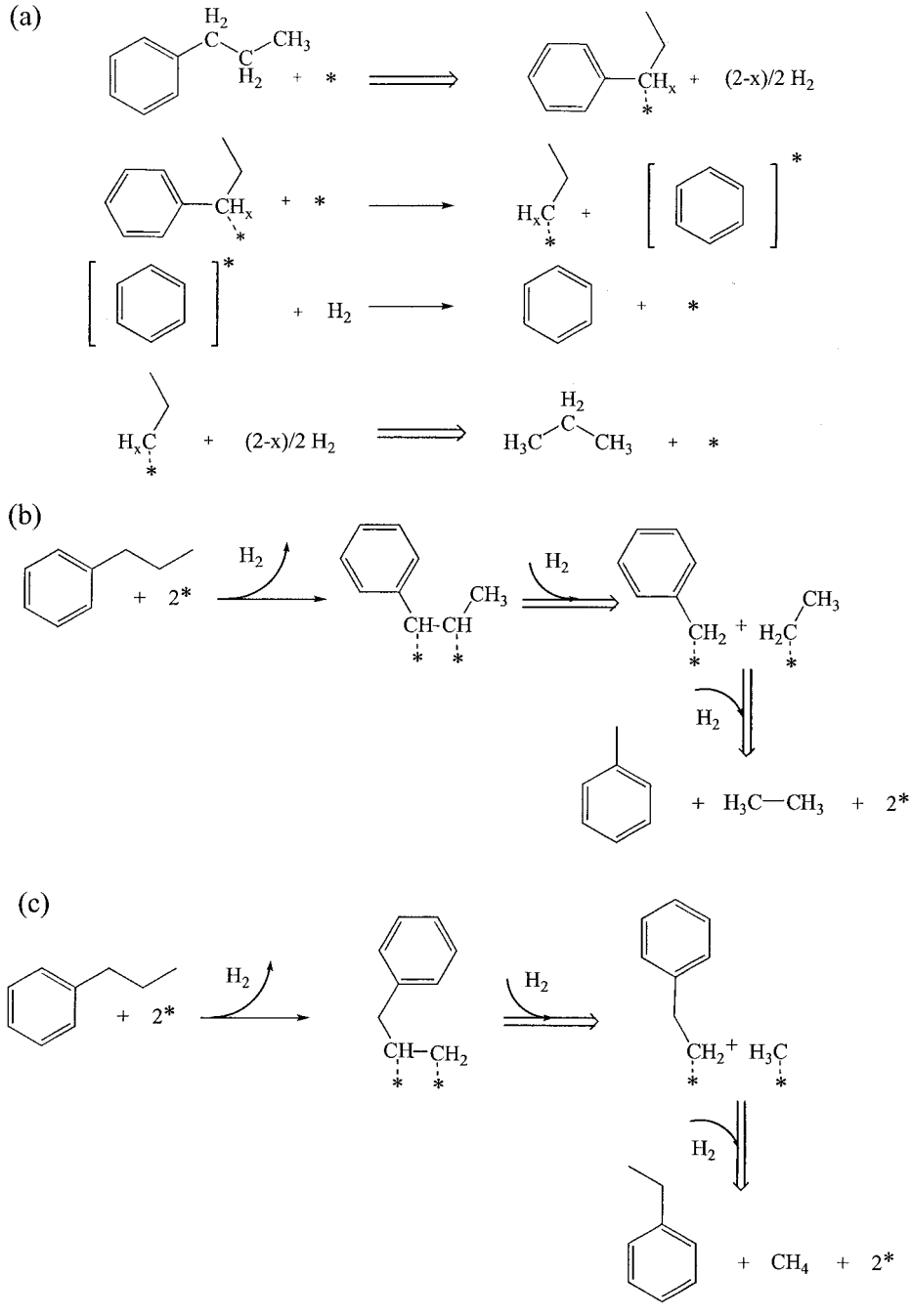

FIG. 10. Elementary step sequences leading to the formation of (a) benzene, (b) toluene, and (c) ethylbenzene. A double arrow and a single arrow represent a global step and an elementary step, respectively.

of 2,6-dimethylpyridine (2,6-DMP) and pyridine carried out over these two materials confirmed the presence of strong and weak Brønsted and Lewis acid sites. Indeed, in agreement with a previous study (31), bands at 1620 and 1650 cm^{-1} (2,6-DMP adsorbed species) were detected for strong and weak Brønsted acid sites, respectively. Similarly, bands at 1625 and 1615 cm^{-1} (pyridine adsorbed species (31)) were observed for strong and weak Lewis acid sites, respectively.

In the case of benzene, *n*-PB was previously isomerised to isopropylbenzene which undergoes cracking (Fig. 11, part a, route 1). Note that isopropylbenzene can also be formed as a final product over a weaker Brønsted acid site than that required for cracking reactions (25, 32). The one-step cracking of *n*-PB leading to benzene might be ruled out because it would involve the formation of the primary carbocationic species $CH_3–CH_2–CH_2^+$. Based on a similar mechanism, the cracking of *n*-PB to toluene and ethylbenzene involves two

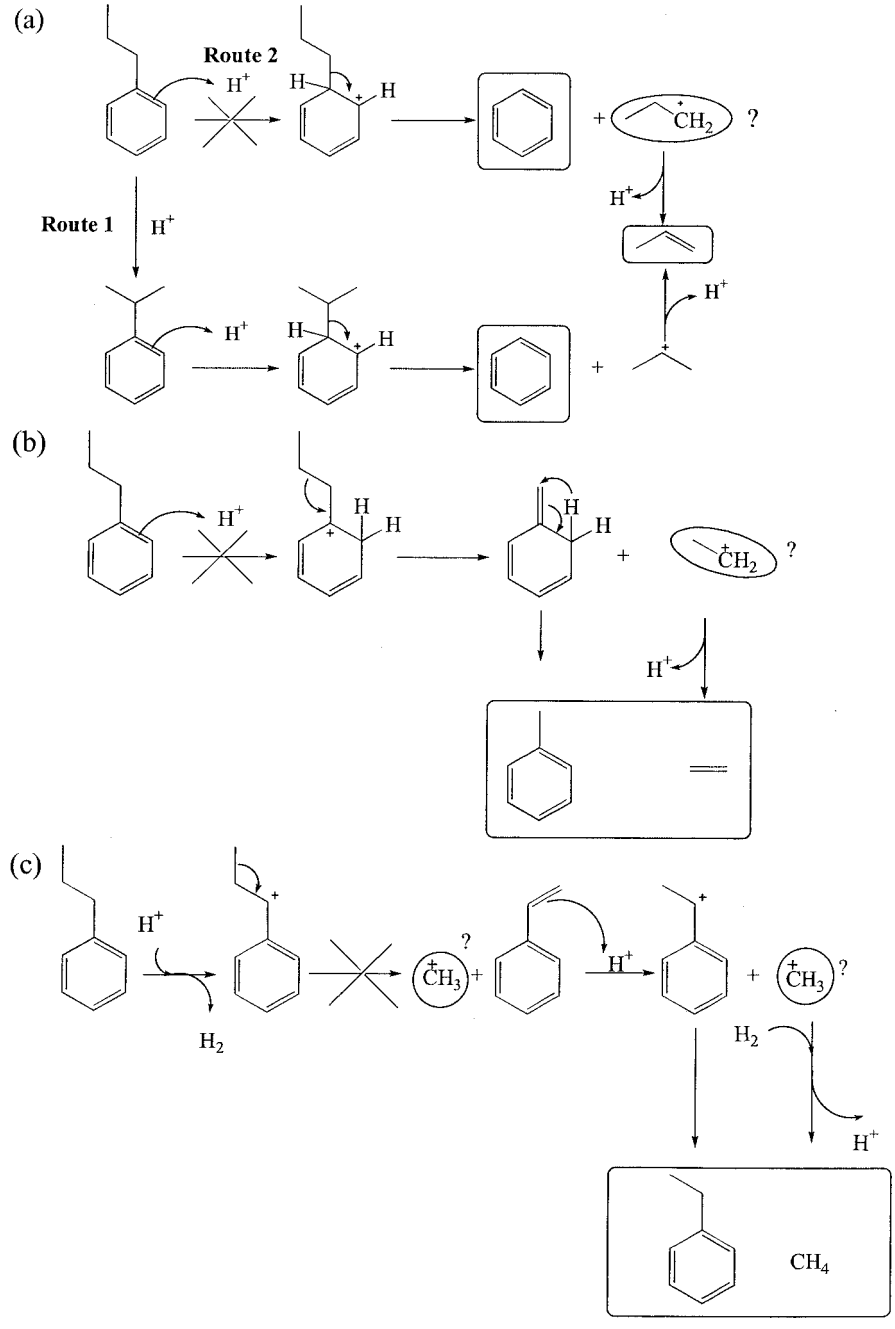

FIG. 11. Cracking through a carbenium ion chain mechanism proposal: (a) benzene, (b) toluene, and (c) ethylbenzene.

comparable thermodynamically unfavoured carbocationic species, CH_3–CH_2^+ and CH_3^+, respectively (Fig. 11, parts b and c).

Thus, the formation of toluene and ethylbenzene is considered to occur through radical mechanisms involving Lewis acid sites (33) which are described in Fig. 12. The radical intermediate species are very stable, especially in the case of the ethylbenzene formation (Fig. 12, part a). Indeed, in this latter case the radical species is stabilised by the aromatic nucleus. Such a mechanism is therefore the most favoured for toluene and ethylbenzene formation. In the case of toluene (Fig. 12, part b), the phenyl propene radical species could desorb as phenyl-2-propene which was not detected under our experimental conditions. For ethylbenzene, the corresponding desorbed products of the phenyl propene radical species (Fig. 12, part a) were observed as *E*- and *Z*-phenyl-1-propene (Fig. 8). Based on the afore mentioned mechanisms, one can finally add that the strength of the Lewis acid sites must reasonably be higher for the formation of toluene than that of ethylbenzene.

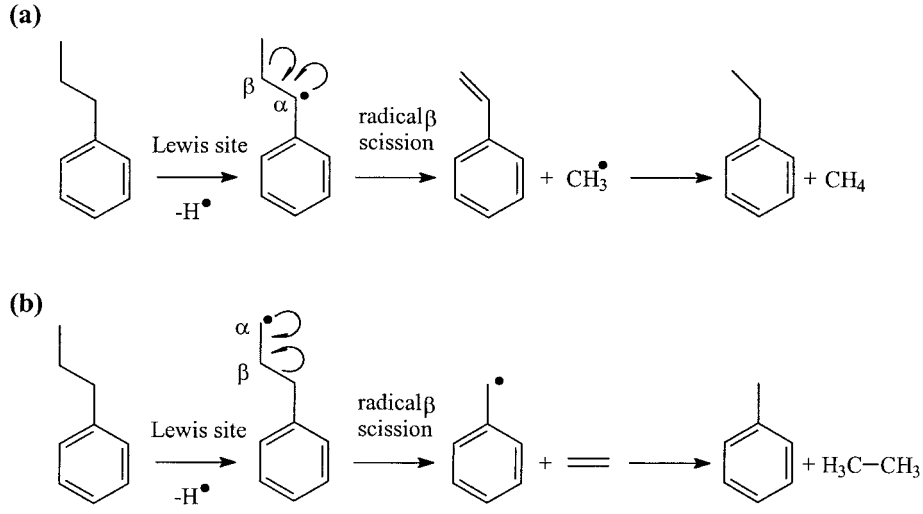

FIG. 12. Cracking through a radical mechanism proposal: (a) ethylbenzene and (b) toluene.

4.2.2. Zero-order reaction with respect to n-PB and kinetics of the hydrodealkylated products. Over 1 wt% Cl–Al_2O_3, the consumption rate of *n*-PB is constant up to 18% conversion (Figs. 8b or 9b). This means, as in the case of hydrogenolysis reactions over platinum, that the surface acid sites are saturated by *n*-PB adsorbed species ($A_{i,ads}$) and a *true* zero-order reaction with respect to the reactant is observed. Even if a degenerated order is considered because of the low conversion of the reactant (less than 10%) over Al_2O_3, a true zero order was assumed considering both the previously described experimental conditions (Sect. 4.1.1.) and the zero order found over the 1 wt% Cl–Al_2O_3 catalyst.

As suggested before (Sect. 4.2.1.), for different acid sites, i.e., weak and strong Brønsted acid sites and weak and strong Lewis acid sites, have to be considered and the balance over the acid sites can therefore be written as follows:

$$[L]_A = [L_1]_A + [L_2]_A + [L_3]_A + [L_4]_A \qquad [8]$$

where $[L]_A$ is the total density of acid sites and $[L_i]_A$ is the partial density of sites saturated by the adsorbed intermediates ($A_{i,ads}$).

From the kinetic data (Fig. 8a), it is obvious that *E*- and *Z*-phenyl-1-propene display an intermediate behaviour over the alumina carrier. According to the proposed mechanism (Sect. 4.2.1.), these intermediates lead to ethylbenzene formation. In the case of the chlorinated alumina, such dehydrogenated intermediates are also observed. However, they do not exhibit the expected intermediate behaviour, notably because of the too low contact times investigated.

In the case of toluene, its corresponding desorbed intermediate (phenyl-2-propene) was not detected. From a kinetic point of view, this suggests that the desorption rate constant is lower than the cracking rate constant.

According to the carbenium mechanism (Fig. 11, part a, route 1), isopropylbenzene is the intermediate that leads to benzene formation over strong Brønsted acid sites. Here it is emphasised that isopropylbenzene does not necessarily undergo cracking when weak Brønsted acid sites are involved. Finally, four reaction products are associated with the four acid sites leading to the three hydrodealkylated products and isopropylbenzene, this latter compound being both an intermediate for the cracking reaction and a final product for isomerisation.

As a consequence, Eqs. [9–11] can be written as follows where k'_1, $k'_{d,i}$, and $k'_{r,i}$ correspond to the adsorption rate constant, the desorption rate constant, and the reaction rate constant over acid sites, respectively:

$$n\text{-PB}_{gas} \xrightarrow{k'_1} A_{i,ads} + H_2 \qquad [9]$$

$$A_{i,ads} \xrightarrow{k'_{d,i}} A_{i,gas} \qquad [10]$$

$$A_{i,ads} \xrightarrow{k'_{r,i}} \text{product}_{i,gas}. \qquad [11]$$

Finally, considering the preceding pathway (Eq. [11]) and the constant formation rate (Fig. 9) of the cracking products, $r'_{product,i}$ can thus be written as follows:

$$r'_{product,i} = k'_{r,i}[A_{i,ads}] = \text{constant} = k'_{r,i}[L_i]_A. \qquad [12]$$

In this equation, $[L_i]_A$ are thus constant, which confirms that all acid sites are saturated. As in the case of the metallic sites (Sect. 4.1.3), the reaction rates are proportional to the number of active acid sites.

4.2.3. Correlation between kinetics and acidic mechanisms from chlorine addition. According to the mechanistic considerations mentioned previously (Sect. 4.2.1.), benzene would preferably be formed over strong Brønsted

acid sites whereas isopropylbenzene would be formed over weaker sites. In addition, toluene would be formed over stronger Lewis acid sites than ethylbenzene.

On the one hand, the formation rate of benzene is increased by a factor of three, whereas the formation rate of isopropylbenzene is almost constant after the addition of chlorine on the alumina carrier (Table 3). Kinetic data thus suggest that the number of strong Brønsted acid sites is significantly enhanced whereas the number of weaker ones remains almost constant. Indeed, Gates *et al.* (34) reported that the addition of chlorine to an alumina carrier enhances the strength of Brønsted acid sites by weakening O–H bonds of adjacent hydroxyls through an inductive effect. Moreover, Berteau and Delmon (35) reported an increase of the total number of Brønsted acid sites.

The increase of the formation rate of benzene after the addition of chlorine to an alumina carrier is therefore in good agreement with the preceding proposed mechanism (Fig. 12, part a) showing that benzene is formed on strong Brønsted acid sites through a carbenium ion chain mechanism. The constant formation rate of isopropylbenzene whatever the catalyst nature (Al_2O_3 or $Cl–Al_2O_3$) suggests that the number of weak Brønsted acid sites remains almost constant, and that the increase in the total number of Brønsted acid sites is mainly due to the increase of the number of strong sites.

On the other hand, the formation rate of toluene increases significantly whereas the formation rate of ethylbenzene decreases slightly over the chlorinated alumina as compared to the alumina carrier (Table 3). These kinetic data are also consistent with our proposed mechanisms suggesting that toluene and ethylbenzene are formed through radical processes involving strong and weak Lewis acid sites, respetively. Indeed, Berteau *et al.* (30) suggested an increase of the electron-deficient state of unsaturated aluminium cations through an inductive effect of chlorine leading to stronger Lewis acid sites. In addition, they reported a slight increase in the number of Lewis acid sites when adding chlorine to an alumina carrier. In the case of Lewis acidity, the increase in the number of strong Lewis acid sites thus mainly occurs at the expense of weak Lewis acid sites since the total number of Lewis acid sites remains almost constant.

5. CONCLUSION

The HDA of *n*-PB was investigated for the first time over model catalysts (Pt/SiO_2, $PtSn/SiO_2$, Al_2O_3, and 1 wt% $Cl–Al_2O_3$ under identical reforming operating conditions (773 K, 5 bars, and $H_2/HC = 5$).

This work allowed us to evaluate separately the contributions of both metallic and acidic functions to HDA reactions. It was found that these reactions occur to a significant extent over both functions through either hydrogenolysis reactions over the metallic catalyst or cracking reactions over the acidic catalyst.

By the use of a C_9 aromatic molecule as reactant, the kinetic study showed that hydrogenolysis and cracking of such a model molecule lead to three hydrodealkylated products (benzene, toluene, and ethylbenzene) through concurrent reactions rather than successive ones as might have been expected at first.

In addition, whatever the nature of the active sites, a true zero-order reaction with respect to *n*-PB was observed over the whole range of contact times used in this study. As a consequence, all the active sites, either metallic or acid ones, were saturated and the reaction rates were determined. As compared to toluene and ethylbenzene, the formation rate of benzene was found to be the highest over the acidic function and the lowest over Pt/SiO_2.

The kinetic study also revealed the intermediates involved in the *n*-PB HDA leading to the corresponding hydrodealkylated products, and mechanisms were suggested to explain their formation. These mechanisms were confirmed by tin promotion in the case of the metallic catalyst and chlorine addition in the case of the acidic one.

As a consequence, over both Pt/SiO_2 and $PtSn/SiO_2$, two types of reaction sequences are proposed: (i) through adsorption on a single site for the formation of benzene, and (ii) through adsorption on two adjacent sites for the formation of toluene and ethylbenzene. Over Al_2O_3 and 1 wt% $Cl–Al_2O_3$, (i) benzene is formed on strong Brønsted acid sites via a carbocationic pathway, and (ii) toluene and ethylbenzene are formed via a radical pathway on strong and weak Lewis acid sites, respectively.

ACKNOWLEDGMENTS

We acknowledge the Institut Français du Pétrole (IFP) for the financial support of this work as well as the ANRT organisation for the CIFRE grant number 128/99 allowed to Ms. S. Toppi. We also thank Dr. C. Marcilly (IFP) for fruitful discussions and for his interest concerning this work. Finally, we gratefully acknowledge Dr. K. Fajerwerg-Sainte-Marie for her kind assistance in FTIR measurements.

REFERENCES

1. Howley, P. A., and Shih, S., U.S. Patent No. 5,001,296 (1991).
2. Wu, A., and Drake, C. A., U.S. Patent No. 5,698,757 (1997).
3. Wu, A., and Drake, C. A., U.S. Patent No. 5,763,721 (1998).
4. Wu, A., and Drake, C. A., U.S. Patent No. 5,945,364 (1999).
5. Grenoble, D. C., *J. Catal.* **51**, 212 (1978).
6. Grenoble, D. C., *J. Catal.* **51**, 203 (1978).
7. Grenoble, D. C., *J. Catal.* **56**, 40 (1979).
8. Duprez, D., Maurel, R., Miloudi, A., and Pereira, P., *Nouv. J. Chim.* **6**, 163 (1982).
9. Kochloefl, K., *in* "Sixth International Congress on Catalysis" (G. C. Bond, P. B. Wells, and F. C. Tompkins, Eds.), Vol. 2, p. 1122. The Chemical Society, London, 1976.
10. Rabinovich, G. L., and Mozhaiko, V. N., *Neftekhimiya* **15**, 373 (1975).
11. Kasaoka, S., Omoto, M., Watanabe, T., and Yakamatsu, K., *Nippon Kagaku Kaishi* **8**, 1418 (1975).

12. Mori, S., and Uchiyama, M., *J. Catal.* **42**, 323 (1976).
13. Duprez, D., Miloudi, A., and Tournayan, L., *Appl. Catal.* **14**, 333 (1985).
14. Kim, C. J., *J. Catal.* **52**, 169 (1978).
15. Beltrame, P., Ferino, I., Forni, L., and Torrazza, S., *Chim. Ind.* **60**, 191 (1978).
16. Beltrame, P., Ferino, I., Forni, L., and Torrazza, S., *J. Catal.* **60**, 472 (1979).
17. Beltrame, P., Casalone, G., Forni, L., Ferino, I., Marongiu, B., and Torrazza, S., *Ind. Eng. Chem. Process Des. Dev.* **23**, 176 (1984).
18. Duprez, D., Pereira, P., Barbier, J., and Maurel, R., *React. Kinet. Catal. Lett.* **13**, 217 (1980).
19. Shephard, F. E., and Rooney, J. J., *J. Catal.* **3**, 129 (1964).
20. Duprez, D., Miloudi, A., Delahay, G., and Maurel, R., *J. Catal.* **90**, 292 (1984).
21. Duprez, D., Miloudi, A., Delahay, G., and Maurel, R., *J. Catal.* **101**, 56 (1986).
22. Boudart, M., and Djéga-Mariadassou, G., "Kinetics of Heterogeneous Catalytic Reactions." Princeton University Press, Princeton, 1984.
23. Humblot, F., Candy, J. P., Le Peltier, F., Didillon, B., and Basset, J. M., *J. Catal.* **179**, 459 (1998).
24. Dautzenberg, F. M., Helle, J. N., Biloen, P., and Sachtler, W. M. H., *J. Catal.* **63**, 119 (1980).
25. Guisnet, M., and Pérot, G., *in* "Zeolite: Science and Technology" (F. R. Ribeiro, A. E. Rodrigues, L. D. Rollman, and C. Naccache, Eds.), p. 397. Nijhoff, The Hague, 1984.
26. Germain, J. E., "Catalytic Conversion of Hydrocarbons." Academic Press, New York, 1969.
27. Sexton, B. A., Hughes, A. E., and Foger, K., *J. Catal.* **88**, 466 (1984).
28. Zhou, Y., and Davis, S. M., *Catal. Lett.* **15**, 51 (1992).
29. Meloni, D., Martin, D., and Guisnet, M., *Appl. Catal. A* **215**, 67 (2001).
30. Berteau, P., Kellens, M. A., and Delmon, B., *J. Chem. Soc., Faraday Trans.* **87**, 1425 (1991).
31. Corma, A., Fornes, V., and Ortega, E., *J. Catal.* **92**, 284 (1985).
32. Baudon, A., Ph.D. dissertation, Université de Poitiers, Poitiers, 1996.
33. Mc Vicker, G. B., Kramer, G. M., and Ziemiak, J. J., *J. Catal.* **83**, 286 (1983).
34. Gates, B. C., Katzer, J. R., and Schuit, G. C. A., "Chemistry of Catalytic Processes." McGraw–Hill, New York, 1979.
35. Berteau, P., and Delmon, B., *Catal. Today* **5**, 121 (1989).